Time resolved ionization measurements with intense ultrashort XUV and X-ray free-electron laser pulses

Victor Tkachenko*,[1,2] Martin Büscher,[1] Hauke Höppner,[1,3] Nikita Medvedev,[4,5] Vladimir Lipp,[2] Giulio Maria Rossi,[2] Flavio Capotondi,[6] Paola Finetti,[6] Emanuele Pedersoli,[6] Ivaylo Nikolov,[6] Mitcho Danailov,[6] Luca Giannessi,[6] Mark J. Prandolini,[7] Sven Toleikis,[8] Katalin Mecseki,[9] Matthew Windeler,[9] Beata Ziaja,[2,10] Franz Tavella,[9] and Ulrich Teubner[1,11]

[1]*Institute for Laser and Optics (ILO), Hochschule Emden/Leer – University of Applied Sciences, Constantiaplatz 4, 26723 Emden, Germany*
[2]*Center for Free-Electron Laser Science CFEL, Deutsches Elektronen-Synchrotron DESY, Notkestrasse 85, 22607 Hamburg, Germany*
[3]*Institute for Radiation Physics, Helmholtz-Zentrum Dresden-Rossendorf e.V., Bautzner Landstrasse 400, 01328 Dresden, Germany*
[4]*Institute of Physics, Czech Academy of Sciences, Na Slovance 2, 18221 Prague, Czech Republic*
[5]*Institute of Plasma Physics, Czech Academy of Sciences, Za Slovankou 3, 18200 Prague, Czech Republic*
[6]*Elettra Sincrotrone Trieste, S.S. 14 km 163,5 in Area Science Park, 34149 Basovizza, Italy*
[7]*Institut für Experimentalphysik, Universität Hamburg, Luruper Chaussee 149, 22761 Hamburg, Germany*
[8]*Deutsches Elektronen-Synchrotron DESY, Notkestrasse 85, 22607 Hamburg, Germany*
[9]*SLAC National Accelerator Laboratory, Sand Hill Rd 2575, CA 94025 Menlo Park, USA*
[10]*Institute of Nuclear Physics, Polish Academy of Sciences, Radzikowskiego 152, 31-342 Kraków, Poland*
[11]*Institute of Physics, Carl von Ossietzky University, Carl-von-Ossietzky-Str. 9-11, 26111 Oldenburg, Germany*

(Dated: February 28, 2019)

Modern free-electron lasers (FEL) operating in XUV (extreme ultraviolet) or X-ray range allow an access to novel research areas. An example is the ultrafast ionization of a solid by an intense femtosecond FEL pulse in XUV which consequently leads to a change of the complex index of refraction on an ultrashort time scale. The photoionization and subsequent impact ionization resulting in electronic and atomic dynamics are modelled with our hybrid code XTANT and a Monte Carlo code XCASCADE. The simulations predict the temporal kinetics of FEL-induced electron cascades and thus yield temporally and spatially resolved information on the induced changes of the optical properties. In a series of experiments at FERMI and LCLS, single shot measurements with spatio-temporal encoding of the ionization process have been performed by a correlation of the FEL pump pulse with an optical femtosecond probe pulse. An excellent agreement between the experiment and the simulation has been found. We also show that such kind of experiments forms the basis for pulse duration and arrival time jitter monitoring as currently under development for XUV-FELs.

I. INTRODUCTION

Free electron laser has been a key for new classes of experiments in the fields of biology, femtochemistry and material science. Examples of free-electron XUV/X-ray lasers include FLASH [1] and XFEL [2] in Germany, FERMI@Elettra [3] in Italy, SACLA [4] in Japan, PAL-XFEL [5] in Korea, and LCLS [6] in the US. These instruments unveiled new horizons in photon science, enabling experiments of a new type and opening new areas in physics. Femtosecond intense FEL pulses trigger ultrafast ionization of solids, which consequently leads to transformation of electronic and atomic structures of the materials. Modification of the dielectric constant of the material implies changes of optical properties as well as phase effects. Changing optical characteristics can be measured by using, e.g., a pump-probe technique with an XUV/X-ray pump and a delayed optical probe. In such a way, the material can be transformed from the initial transparent state to an opaque state. Thus, a gate is created, which is further referred to as an 'optical gate'. This gate reflects visible and infrared light. Due to the very fast ionization dynamics in solids, formation of such an optical gate may take less than 10 fs following the Keldysh model [7, 8]. This is faster than the Kerr gate which is limited by the pulse duration [8]. Creation and introduction of such an ultrafast optical gate are the goals of XUV-PUMA project. The ultrafast optical gate, in its turn, will be a basis for

* Corresponding authors: V. Tkachenko (victor.tkachenko@desy.de) and U. Teubner (ulrich.teubner@hs-emden-leer.de)

the 'timing tool', which will give an opportunity to measure the pulse arrival time, to characterize the pulse structure and to monitor the jitter of XUV- and X-ray FEL pulses.

II. MODELS AND EXPERIMENTS

For modelling electronic and atomic time dependent dynamics, we use our in-house codes XCASCADE (X-ray-induced electron cascades) [9] and XTANT (X-ray thermal and non-thermal transitions) [10, 11]. XCASCADE is a Monte-Carlo code which simulates electronic cascades in irradiated materials. An event-by-event Monte-Carlo scheme averages over many trajectories to gather reliable statistics. These events may include photoexcitation of hot electrons, decay of inner-shell holes, elastic and inelastic collisions of electrons with atoms. XCASCADE uses predefined atomistic cross-sections for these processes. The material is supposed to be exposed to relatively low fluence radiation that does not produce substantial damage and preserves quasineutrality during the electron cascading. It is a versatile tool which can be applied to any material (within the abovementioned atomic approximation).

An XCASCADE-3D is an extension [12] of XCASCADE, which also tracks electronic cascades in space with 3D-resolution. Thus, the effect of fast electron transport can be estimated. With the spatial and temporal estimation of the electron density, the optical properties using the Drude model can be calculated.

The XTANT code keeps XCASCADE principles of Monte-Carlo based trajectory constructions for high-energy electrons, but it also treats low-energy electrons within the valence band and bottom of the conduction band by using temperature rate equations. Usage of the tight binding model allows to resolve a transient band structure of the material at each time step and thus, by calculating a potential energy surface, we obtain the atomic forces and, subsequently, molecular dynamics in the material. In such a way, changes in the atomic trajectories are also available. The nonadiabatic electron-ion coupling is traced with the Boltzmann collision integral. Furthermore, transient optical properties of the material can be calculated either with the RPA (random phase approximation) or the Drude approach [13]. The tight binding parameterization in the current version of XTANT is restricted to carbon, silicon and gallium arsenide [14, 15], although a new version of XTANT being developed now includes a more universal parameterization scheme for numerous materials. A simplified scheme of XTANT modules is shown in Fig. 1.

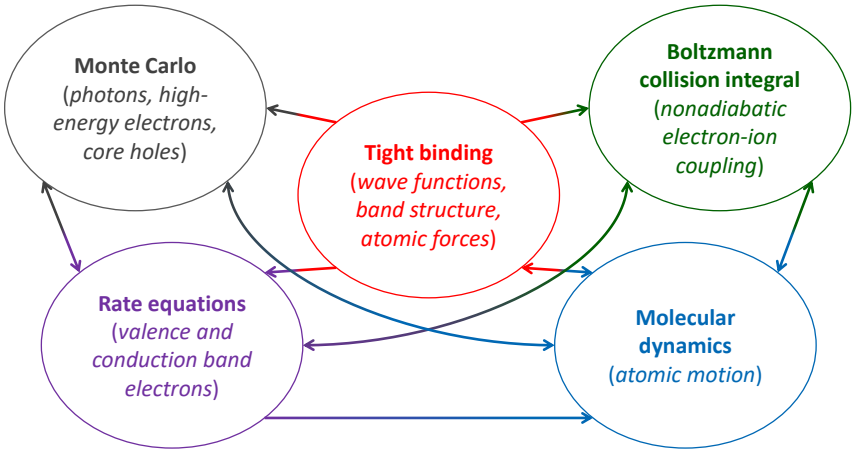

FIG. 1: Scheme of the modules of the XTANT code and connections between them. Figure reproduced from Ref. [11].

To conclude, XCASCADE and XTANT serve as tools for modelling ionization dynamics in solids irradiated with XUV/X-ray pulses. Calculation of transient optical properties such as reflectivity, transmissivity or temporal phase, which are typically measured with the pump-probe technique, gives an opportunity to compare results of simulations directly with time resolved experiments. We have tested the validity of the XTANT model on published experiments with diamond and silicon where optical pump radiation was used to create transient non-equilibrium states of the materials [13]. With modern tools at FELs, it became possible to make single-shot experiments with optical or X-ray probe and time resolution down to 10 fs [16–18].

An example of such an experiment was performed at FERMI@Elettra in 2016 by Franz Tavella et al [19]. A polycrystalline diamond sample was exposed to the soft X-ray pulses of photon energy $E_{\text{phot}} = 47.4$ eV. Then it was probed by an optical pulse with a wavelength $\lambda = 630$ nm. The time resolution of the experiment did not exceed 10 fs. The result was a detection of a solid-to-solid nonthermal transition of diamond into graphite on a time scale of 150

fs which is one of the fastest phase transitions ever observed. Non-thermal graphitization had been observed earlier by Gaudin et al. [20], but not in a time-resolved mode, and theoritically described by Medvedev et al. [10].

The local dose absorbed by the material should be at least 0.7 eV/atom to cause graphitization. The mechanism of such a phase transition includes very fast electronic excitation from the valence to the conduction band (within a few femtoseconds for XUV case) followed by a diamond band gap collapse and further atomic relocation to new equilibrium positions corresponding to overdense graphite. All stages of this transformation were followed by experimental measurements of a transmission signal as well as by XTANT simulation of transient transmission, found in excellent agreement with each other. Further confirmation of actual graphitized final state was made by post-mortem analysis of the sample, which included scanning probe microscopy, confocal Raman micro-spectroscopy and X-ray photoelectron spectroscopy. Different experimental fluences resulted in different observed graphitized layers in the targets. A finite transmission coefficient was higher in samples with a thinner graphitized layer (Fig. 2). The dependence of the layer thickness on a transmission coefficient was accounted in XTANT by adding relaxation time approximation for electronic relaxation. This simplified model assumed linear dependence of an affected layer thickness, evolving from the attenuation layer, on a probe time delay.

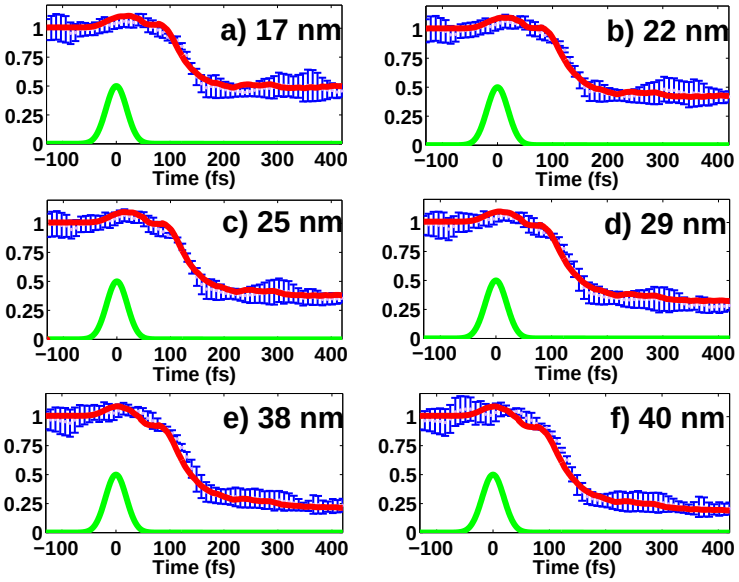

FIG. 2: Transmission signal observed experimentally (error bars) and simulated with XTANT (solid lines) from XUV irradiated diamond for various transient graphite layers at 400 fs. FEL photon energy $E_{\mathrm{phot}} = 47.4$ eV, FEL pulse duration $\tau_{\mathrm{FEL}} = 52.5$ fs, probe pulse wavelength $\lambda = 630$ nm.

A number of other interesting modelled effects has also been recently observed with XTANT. One of the best studied examples is melting of silicon. Depending on the absorbed dose from the FEL pulse, solid silicon which has a diamond-like crystal lattice can either transform into the low density liquid (LDL) through a thermal channel (Fig. 3) or into the high density liquid (HDL) through a primarily non-thermal channel (Fig. 4). The thresholds are estimated to be ~ 0.65 eV/atom for thermal melting and ~ 0.9 eV/atom for non-thermal melting [11, 21]. The presence of the LDL or HDL phase in a simulation can be resolved by the positions of silicon atoms and interatomic bonds or by a characteristic powder diffraction pattern. The mechanism of the thermal melting transition is attributed to non-adiabatic electron-ion coupling when hot electrons transfer its energy to the lattice, heating and transforming it. The mechanism of non-thermal melting is identical to the non-thermal graphitization case: if the density of electrons in the conduction band is sufficiently high, a change of the interatomic potential and band gap shrinking before the heating of the crystal lattice may be induced.

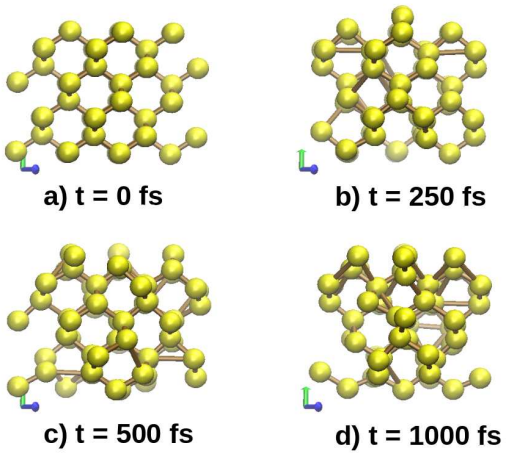

FIG. 3: Snapshots of silicon being irradiated by the FEL pulse with 0.66 eV/atom absorbed dose, photon energy $E_{\text{phot}} = 50$ eV, $\tau_{\text{FEL}} = 10$ fs.

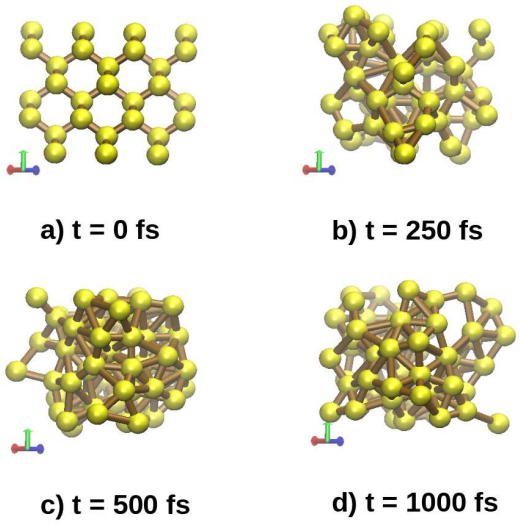

FIG. 4: Snapshots of silicon being irradiated by the FEL pulse with 1.78 eV/atom absorbed dose, photon energy $E_{\text{phot}} = 50$ eV, $\tau_{\text{FEL}} = 10$ fs.

Another modelled example, related to silicon, is ablation. The threshold for this process was predicted to be ~ 2.6 eV/atom [11]. Absorption of such a dose results in at least 12 % of valence electrons in the conduction band and electronic temperature of ~ 20 kK. The material disintegrates, and single atoms and small molecular fragments are expected to be observed. The ablation goes via the non-thermal melting mechanism on a subpicosecond timescales through the HDL phase (Fig. 5).

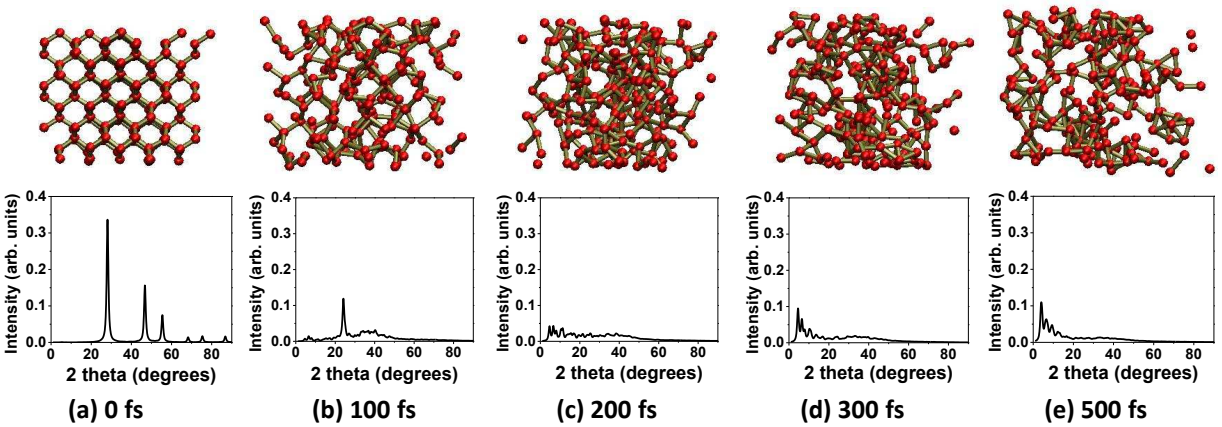

FIG. 5: Snapshots of silicon being irradiated by the FEL pulse with 3 eV/atom absorbed dose, photon energy $E_{\rm phot}$ = 92 eV, $\tau_{\rm FEL}$ = 10 fs. Corresponding simulated powder diffraction patterns are obtained for X-ray photons of 1.54 Å. Figure is reproduced from Ref. [11].

Similar disintegration is observed in amorphous carbon (a-C) at doses above $\sim$ 0.85 - 0.9 eV/atom [11]. The spallation of a-C goes through graphitization on a timescale of a few picoseconds. As a result, the material is fragmented, forming separate clusters (Fig. 6). That distinguishes it from ablation when single atoms or few-atomic species are removed from the bulk.

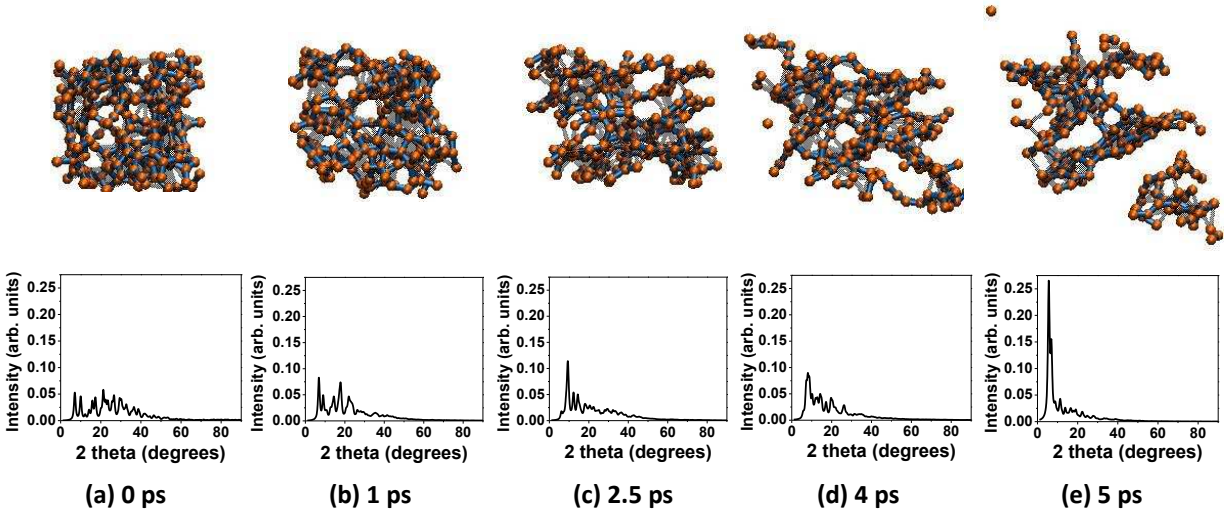

FIG. 6: Snapshots of amorphous carbon being irradiated by the FEL pulse with 1 eV/atom absorbed dose, photon energy $E_{\rm phot}$ = 92 eV, $\tau_{\rm FEL}$ = 30 fs. Corresponding simulated powder diffraction patterns are obtained for X-ray photons of 1.54 Å. Figure is reproduced from Ref. [11].

At extremely intense FEL irradiation, ultrafast atomic disorder leads to the warm dense matter formation on a timescale of few tens of femtoseconds. Diamond, absorbing a dose between $\sim$ 18 and 25 eV/atom, transiently undergoes melting through a very quick graphite-like state which lasts only a few fs [22] (Fig. 7). Such a process can be considered almost purely non-thermal, since it is too fast for non-adiabatic effects to contribute, as was confirmed by a separate simulation done within the Born-Oppenheimer approximation framework.

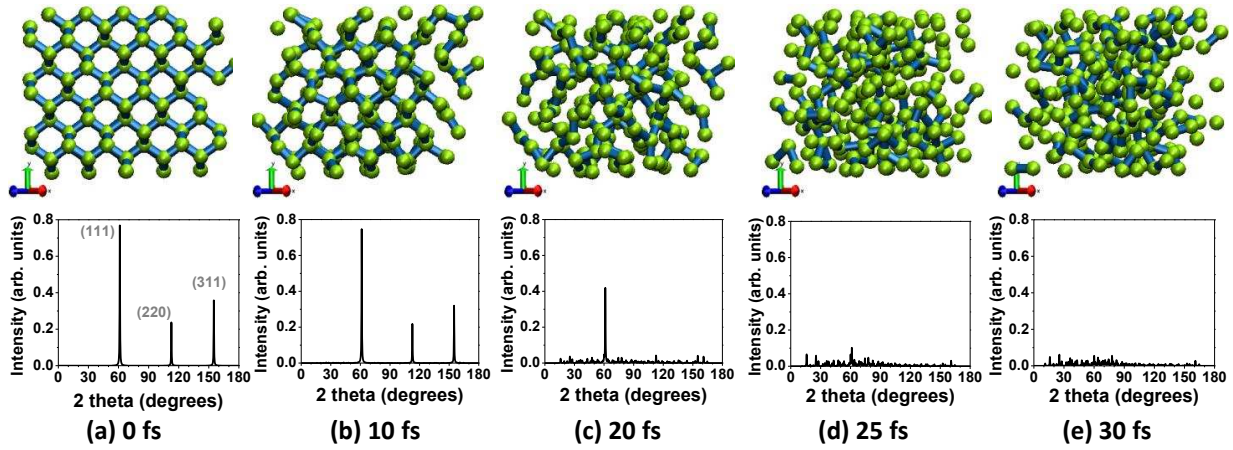

FIG. 7: Snapshots of diamond being irradiated by the FEL pulse with 18.5 eV/atom absorbed dose, photon energy $E_{\text{phot}} = 6100$ eV, $\tau_{\text{FEL}} = 10$ fs. Corresponding simulated powder diffraction patterns are obtained for X-ray photons of 1.54 Å. Figure is reproduced from Ref. [11].

The XCASCADE code is also efficient for calculations in a regime of excitation below damage threshold, when the atomic rearrangement insignificantly affects the optical properties within the cascade duration. Such an experiment, aiming to study electron cascades in a solid, was conducted at LCLS in 2017 by Katalin Mecseki et al [23]. Samples of Si_3N_4, Si and SnO_2 were irradiated with approximately 20 fs FWHM FEL pulse at 5 keV and 9 keV photon energies arriving at 30° to the target. Simultaneously, they were probed by an ultrashort ($\tau < 10$ fs) optical pulse at $\lambda = 800$ nm at a normal incident angle and the transmission signal was decoded. By measuring the transmission of a sample, the electron dynamics and free electron density were analyzed via changes of the complex index of refraction.

Such measurements in optical cross-correlation experiments allow for diagnostics of the X-ray FEL pulse, namely its arrival time and duration. The perfect 'timing tool' material should be highly transparent for the X-ray radiation and also sensitive to an optical pulse [9]. Then the impact of an X-ray pulse to the experimental setup is minimized and detection of optical response to the ionization dynamics is feasible.

Both, experimental observations and XCASCADE demonstrated faster electron kinetics and ionization in SnO_2 compared to Si_3N_4 and especially to Si (not shown) (Fig. 8). The effect is even more pronounced at $\hbar\omega = 9$ keV, as the L-shell ionization potential approximately equals to $I_p = \hbar\omega/2$. As a result, saturation of the electron density takes less than 50 fs. Measuring transient transmission and calculating its derivative were followed by the direct time domain deconvolution of the laser pulse duration which yielded the material response to the FEL pulse. These results were also in agreement with the modelling.

As we already mentioned, the XCASCADE-3D code allows to trace X-ray/XUV-induced cascades in 3-dimensional space, which is a significant improvement compared to the original XCASCADE code, providing only temporal resolution. Based on the common roots and similar programmistic structure of XCASCADE-3D and XTANT codes, another challenging idea is to combine the advantages of the both codes. XTANT code is capable of calculating optical properties from the electronic band structure within the RPA model [13, 24], which is a more precise estimation than the Drude model implemented in XCASCADE-3D [13]. In addition, XTANT does not have any spatial resolution. Using the spatially resolved cascading information from XCASCADE-3D, XTANT can then calculate optical coefficients within a particular chosen layer of the material. Temporal distribution of electrons in the material may become very non-uniform because of fast ballistic transport and diffusion effects. In Fig. 9 examples of the temporal and spatial electron energy density distribution in silicon nitride calculated by XCASCADE-3D are shown for the cases of XUV ($\hbar\omega = 50$ eV) and hard X-ray ($\hbar\omega = 9000$ eV) irradiation. The calculations take into account both elastic and inelastic collisions of electrons on atoms. The plots are averaged over tens of thousands of cascades. The electrons are stopped after their kinetic energy falls below 8.15 eV. Hard X-ray photons excite electrons to higher energies, and created core shell holes also decay via Auger process, cascading in this case lasts significantly longer than in the case of XUV. Additionally, the longitudinal electron range in the case of X-ray is much larger due to the higher photon attenuation depth and electron ballistic transport.

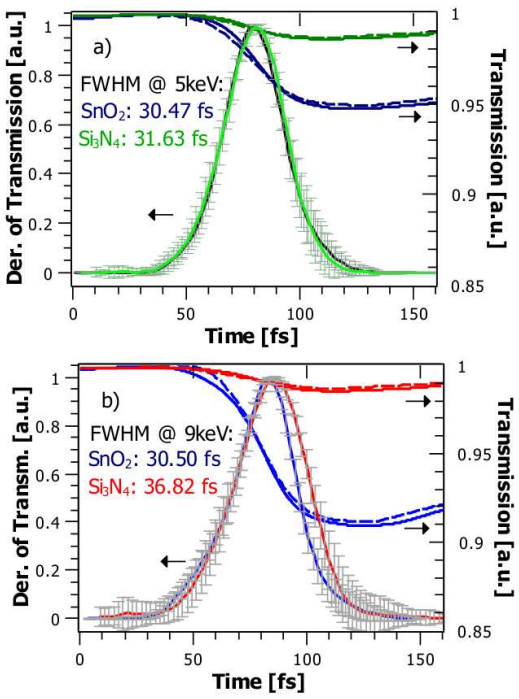

FIG. 8: Measured (solid lines) and calculated (dashed lines) single shot and averaged transmission and the derivative of the measured transmission of SnO_2 (blue lines) and Si_3N_4 (green and red lines) at photon energies 5 keV (a) and 9 keV (b). Figure is partly reproduced from Ref. [23].

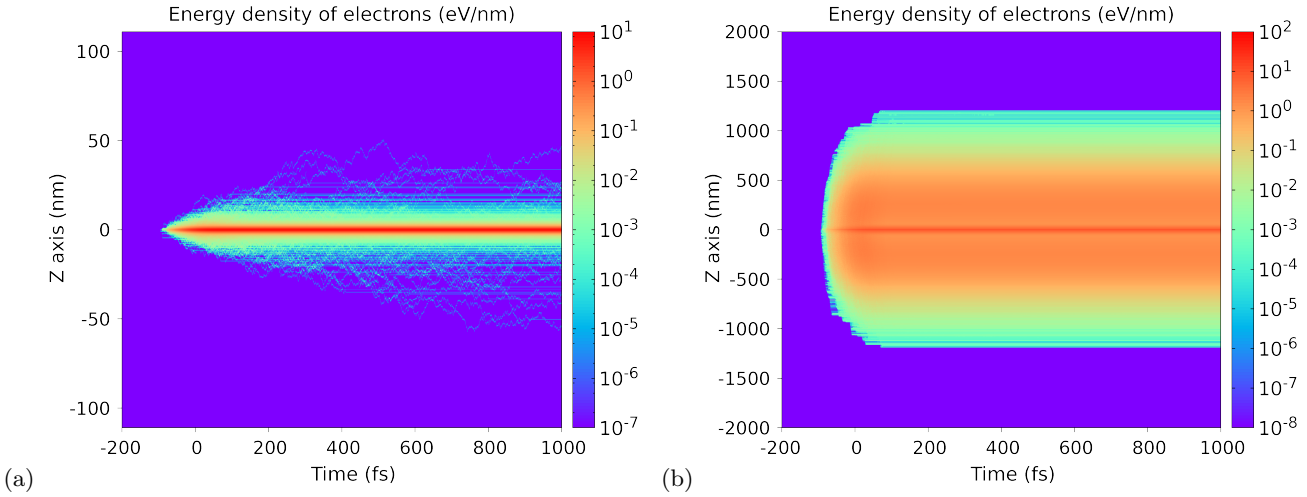

FIG. 9: Calculated spatial and temporal distribution of electron energy density in XUV, 50 eV (a), and X-ray, 9000 eV, (b) irradiated Si_3N_4 sample, pulse duration $\tau = 74.9$ fs. Propagation of electrons in z direction deeply into the bulk of the material is taken into account. The point $z = 0$ corresponds to the position in which a single photon was absorbed (probable from surface to the attenuation depth of the material). The point $t = 0$ corresponds to the center of the FEL pulse.

An idea of the ionization based 'timing tool' we mentioned, was presented in [8]. Therein, the probe pulse and its spectral properties were characterized. However, in our FEL-related studies, the original experimental setup is modified to match our requirements. The pump pulse, which initializes effects and changes in a sample, is produced by the FEL. The ultrashort infrared probe is produced by a NOPA (non-collinear optical parametric amplifier) and

well characterized independently. The IR-pulse from the NOPA obviously cannot serve as a pump for the XUV FEL probe pulse. In such a way, an XUV pump is investigated and characterized from correlation measurement with the IR-pulse. The temporal axis of the single-shot experiment is encoded spatially into the ionization structure on the sample which then is imaged onto a CCD camera. In order to get a single-shot diagnostic, the wavefront of the FEL pulse is tilted with respect to the target. The arrival time of each portion of the pulse is then defined by the spatial positions on the sample [18, 25]. The sketch of the complete experimental setup is shown in Fig. 10. This setup allows to characterize a single FEL pulse in time and frequency domains, as particularly it was demonstrated in [18].

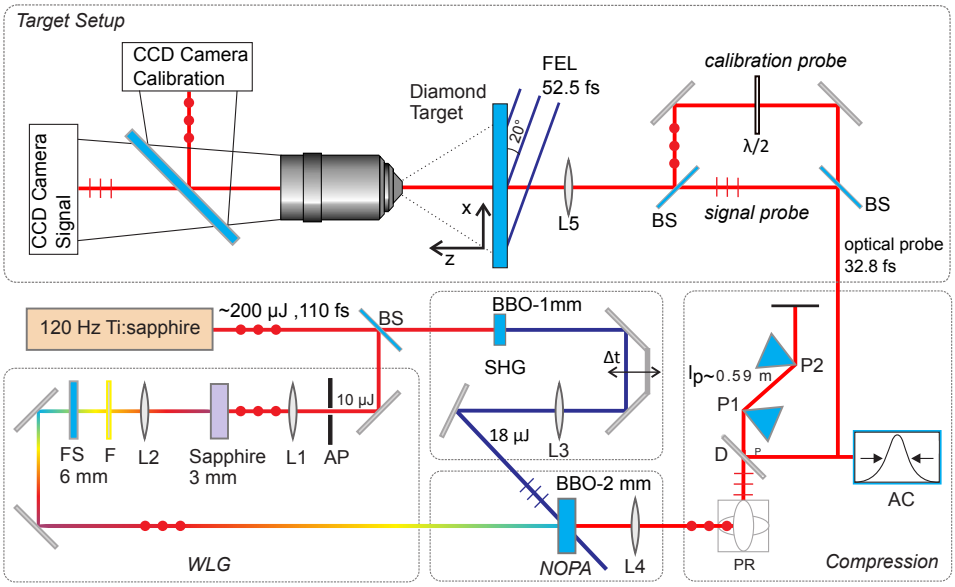

FIG. 10: Scheme of the XUV pump - optical probe correlation experimental setup.

III. CONCLUSIONS

Ultrafast ionization of solid samples by ultrashort wavelength FEL pulses has been investigated at various conditions. The results show that, depending on the energy and the intensity of an FEL pulse, the ionization process can be either used as a 'timing tool' to diagnose temporal properties of the FEL pulse, or, alternatively, as an instrument to induce various phase transitions in the target.

The material modifications strongly depend on the absorbed X-ray or XUV dose. Phase transitions such as solid-to-solid, solid-to-liquid, ablation, spallation, or warm dense matter formation can be observed. A notable example of the XFEL induced phase transition is the ultrafast non-thermal graphitization of diamond, which has been identified in both experiment and simulations. It has been shown that this process is faster than any known non-thermal melting transition which requires at least $\sim 300 - 500$ fs.

At relatively low intensities and high photon energies, electron cascading may occur. As observed in experiments, this may have a strong influence on pulse duration measurements. However, by choosing a suitable target material for a particular photon energy, cascading time may be shortened. This is important for 'timing tool' diagnostics based on the described method. For example, it was shown that SnO_2 is a suitable material for the pulse diagnostics at 5 keV photon energy. Then, in comparison to other (standard) materials, the cascading time in it is significantly reduced and thus improves the accuracy of the measurements.

The present work shows that our in-house codes XTANT and XCASCADE, dedicated to a prediction of the photon-matter interaction in the range from XUV to hard X-ray, are capable of producing accurate results. Experimental results for graphitization and electron cascades in target materials successfully confirmed the validity of the codes.

IV. ACKNOWLEDGEMENTS

V.T., U.T. and M.B. acknowledge funding from the German Ministry of Education and Research (BMBF project no. 05K16ME1). N.M. acknowledges partial financial support from the Czech Ministry of Education, Youth and

Sports, Czech Republic (Grants LTT17015 and LM2015083).

V. REFERENCES

[1] S. Schreiber and B. Faatz. The free-electron laser FLASH. *H. Pow. Las. Sci. and Engin.*, 3:e20, 2015.
[2] M. Altarelli. The European X-ray free-electron laser facility in Hamburg. *Nucl. Instr. and Meth. in Phys. Res. Sec. B: Beam Interactions with Materials and Atoms*, 269(24):2845–2849, 2011.
[3] E. Allaria et al. Highly coherent and stable pulses from the FERMI seeded free-electron laser in the extreme ultraviolet. *Nat. Phot.*, 6(10):699–704, 2012.
[4] D. Pile. X-rays: First light from SACLA. *Nat. Phot.*, 5(8):456–457, 2011.
[5] H.S. Kang et al. Hard X-ray free-electron laser with femtosecond-scale timing jitter. *Nat. Phot.*, 11(11):708–713, 2017.
[6] P. Emma et al. First lasing and operation of an ångstrom-wavelength free-electron laser. *Nat. Phot.*, 4(9):641–647, 2010.
[7] L.V. Keldysh. Ionization in the field of a strong electromagnetic wave. *Sov. Phys. - JETP*, 20(5):1307, 1965.
[8] U. Teubner, U. Wagner, and E. Förster. Sub-10 fs gating of optical pulses. *J. Phys. B: At. Mol. Opt. Phys.*, 34:2993–3002, 2001.
[9] N. Medvedev. X-ray-induced electron cascades in dielectrics modeled with XCASCADE code: Effect of impact ionization cross sections. *Appl. Phys. B*, 119:417, 2015.
[10] N. Medvedev, H.O. Jeschke, and B. Ziaja. Nonthermal phase transitions in semiconductors induced by a femtosecond extreme ultraviolet laser pulse. *New J. Phys.*, 15:015016, 2013.
[11] N. Medvedev et al. Various damage mechanisms in carbon and silicon materials under femtosecond X-ray irradiation. *4open*, 1:3, 2018.
[12] V. Lipp, N. Medvedev, and B. Ziaja. Classical Monte-Carlo simulations of x-ray induced electron cascades in various materials. *SPIE + Optoelectr. Proc.*, 2017.
[13] V. Tkachenko et al. Transient optical properties of semiconductors under femtosecond x-ray irradiation. *Phys. Rev. B*, 93:144101, 2016.
[14] V. Tkachenko, N. Medvedev, and B. Ziaja. Transient changes of optical properties in semiconductors in response to femtosecond laser pulses. *Appl. Sci.*, 6(9):238, 2016.
[15] V. Tkachenko, N. Medvedev, V. Lipp, and B. Ziaja. Picosecond relaxation of X-ray excited GaAs. *High En. Dens. Phys.*, 24:15–21, 2017.
[16] T. Maltezopoulos et al. Single-shot timing measurement of extreme-ultraviolet free-electron laser pulses. *New J. Phys.*, 10:033026, 2008.
[17] M. Harmand et al. Achieving few-femtosecond time-sorting at hard X-ray free-electron. *Nat. Photonics.*, 7:215, 2013.
[18] P. Finetti et al. Pulse duration in seeded free-electron lasers. *Phys. Rev. X*, 7:021043, 2017.
[19] F. Tavella et al. Soft x-rays induce femtosecond solid-to-solid phase transition. *High En. Dens. Phys.*, 24:22–27, 2017.
[20] J. Gaudin et al. Photon energy dependence of graphitization threshold for diamond irradiated with an intense XUV FEL pulse. *Phys. Rev. B*, 88:060101, 2013.
[21] N. Medvedev, Z. Li, and B. Ziaja. Thermal and nonthermal melting of silicon under femtosecond x-ray irradiation. *Phys. Rev. B*, 91:054113, 2015.
[22] N. Medvedev and B. Ziaja. Multistep transition of diamond to warm dense matter state revealed by femtosecond X-ray diffraction. *Sci. Rep.*, 8(1):5284, 2018.
[23] K. Mecseki et al. Hard X-ray induced fast secondary electron cascading processes in solids. *Appl. Phys. Lett.*, 113:114102, 2018.
[24] F. Trani, G. Cantele, D. Ninno, and G. Iadosini. Tight-binding calculation of the optical absorption cross section of spherical and ellipsoidal silicon nanocrystals. *Phys. Rev. B*, 72:075423, 2005.
[25] H. Höppner. *Optical Parametric Chirped Pulse Amplifiers for Seeding, Pulse Metrology and Science at Free-Electron Lasers*. PhD thesis, University of Oldenburg, 2018.